A Multiple Quantum Well Structure Simulator

Becer Zoubir
Faculty of Art, Science and Technology
University of Northampton
Northampton, UK
University of Eloued
Eloued, Algeria.
e-mail: zoubir.becer@northampton.ac.uk

Abdeldjalil Bennecer
Faculty of Art, Science and Technology
University of Northampton
Northampton, UK
e-mail: abdeldjalil.bennecer@northampton.ac.uk

Nouredine Sengouga
Faculty of Exact Sciences
University of Biskra
Biskra, Algeia
e-mail: n.sengouga@univ-biskra.dz

***Abstract*— A simulator was developed for modeling and designing multiple quantum wells structures such as quantum well infrared photodetectors and quantum cascade laser, based on a single-electron effective mass Schrödinger equation. It employs box integration finite differences and transfer matrix approaches to find energies of bound and scattering states in the structures. The graphical user interface allows the user to vary easily design parameters including effective mass, layer thickness and number of layers as well as simulation parameters in order to optimize the structure for different device applications and functionality. Three simulation examples were performed on: three coupled quantum wells structure, two-color asymmetric quantum well infrared photodetector structure and on a quantum cascade laser design. The results show an accuracy which is comparable to more complicated simulations.**

Keywords - Effective mass approximation; Multiple Quantum Wells Structures; FDM; TMM

I. INTRODUCTION

Recent advances in semiconductor device and technology has posed new requirements on methods and tools for the simulation of semiconductor heterostructure device. At this device technology level, quantum effects are very important as devices critical sizes reduce to a few nanometers, and then many of the classical assumptions become invalid and must be discarded in favour of a more quantum mechanical description [1]. Importantly, such kind of structures has useful electronic and optoelectronic properties and interestingly, are still drawing a lot of attention [2]. This has driven remarkable progress in intersubband device physics which showed in the realisation of many Quantum devices namely Quantum Well Infrared Photodetectors (QWIPs), Cascade Lasers (QCLs) and Type II superlattice infrared photodetectors [2]. One difficulty of modelling heterostructures is the accurate determination of the energy levels and wave functions of carriers in these structures which became sensitive to the input parameters (effective masses and band gap energies) when modelling narrow gap materials such as InAs and InSb [3]. Another difficulty of modelling heterostructures is the determination of valence band offset (VBO) which is generally available from literature but there are large discrepancies around reported values due to the imperfection of heterointerfaces [4]. Variation in the VBO creates a significant fluctuation in the modelled outcomes for narrow-gap materials.

Several Commercial TCAD tools such as ISE-TCAD®, APSYS® and SILVACO® and software packages exist that are able of addressing different device geometries, different degrees of quantum confinement and different transport regimes [5]. Some of these tools suffer from complexity and are in fact a collection of specialized models tailored to specific tasks and offer little flexibility. Others need significant research efforts in semiconductor and quantum physics from the user to operate them properly.

The purpose of this work is to provide one dimensional numerical simulations of multiple quantum wells devices using a simple, flexible and highly efficient simulator– MQWSS: Multiple Quantum Well Structure Simulator. The main MQWSS graphical user interface is shown in Fig.1. The MQWSS simulator is based on the effective mass approximation, which allows to solve the Schrödinger equation under the assumption of envelope function [6]. From the solution of Schrödinger equation, the absorption peaks are calculated automatically and can be controlled by adjusting layers' widths and applied electric field. This offers an insight to the user to intuitively align energy bands edge in real time and with reasonable accuracy before carrying a full load computation in multiple quantum well structure based devices.

Besides what it is originally designed for, the program can be used as an interactive educational tool to learn about quantum phenomena in heterostrucures such miniband formation in superlattices and quantum wells interaction.

0-7695-6405-4/18/$31.00 ©2018 IEEE
DOI 10.1109/UKSim.2018.00044

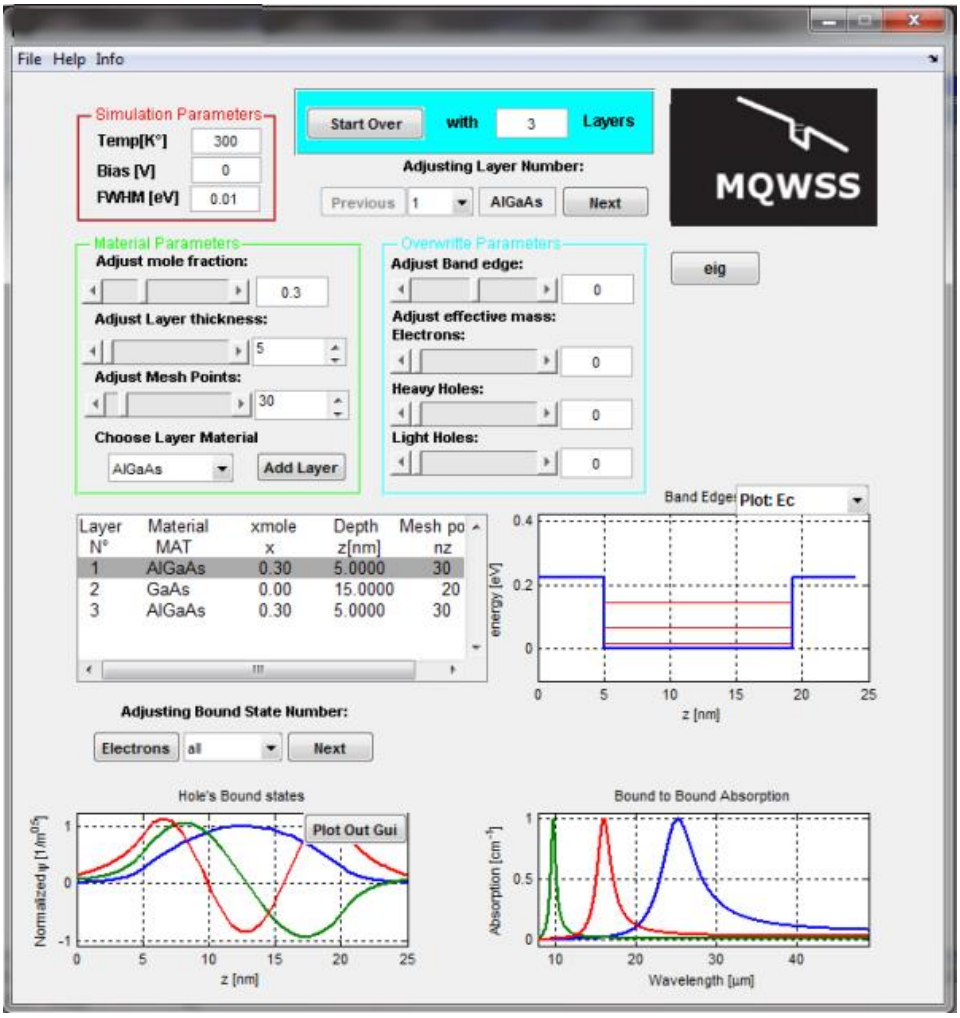

Figure 1. The main MQWSS usser interface with a set of instructions implementing an AlGaAs/GaAs/AlGaAs heterostructure.

In the following sections three application examples are provided: 1) a structure of three coupled quantum wells, 2) a two-color asymmetric quantum well infrared photodetector design and 3) a quantum cascade laser design.

II. SIMULATION APPROACH

Nowadays, heterostructures are the primary construction components of most advanced semiconductor devices being manufactured. They are required elements for highest performance optoelectronic detectors and sources [7]. The advantage of using heterostructures is that they enable precise control over the states of motions of electrons and holes in semiconductors devices [7]. A naive heterostructure comprises of a single heterojunction, which is boundary surface within a semiconductor crystal across which the conduction or/and valence bands edges usually do not line up. Boundary surfaces between GaSb and InAs and between GaAs and AlGaAs semiconductors are examples of such heterojunctions. Fig.2 shows the three different types of heterojunctions and explains how the energy band edges are alignment in the nearly matched InAs/GaAs/AlSb material system [8], [9]. Most devices such as Quantum Well Infrared Photodetector, type II Superlattices detectors, Quantum Cascade Lasers include more than one heterojunction, and are thereby more appropriately named by the more general word heterostructure. The conduction or/and band offset is the basis for the marked and varied behaviour of such devices.

Semiconductor devices performances can be improved using heterostructures which allow the device engineers to locally adjust the energy-band edges' alignment of the semiconductors and thus guide the movements charge carriers. Once a planar heterostructure is formed, a multiple potential quantum wells of different shapes are created and so the carriers find themselves prevented to move in some direction usually the growth direction. In such wells, its energies become discrete and differ from those observed in bulk materials.

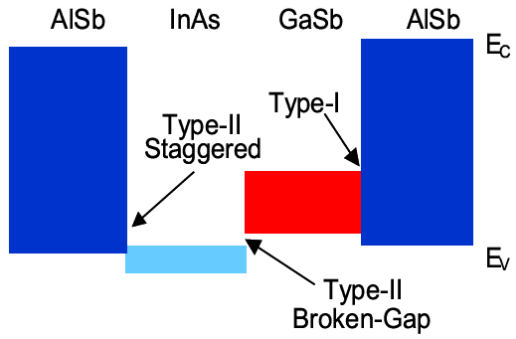

Figure 2. Schematic representation of the band alignments in the nearly matched InAs/GaAs/AlSb material system. The solid rectangles indicate the relative position of energy gaps and band edges of the different material among each other [8], [9].

The MQWSS is based on a single band effective mass approximation. This is a good approximation for bound energies near conduction, heavy hole and light hole band edges. This approximation decomposes the wave function into an atomic-scale part and a more slowly varying envelope function:

$$\Phi(\mathbf{r}) = u_{c,v}(\mathbf{r}) e^{i\mathbf{K}_{//}^{c,v}\mathbf{r}_{//}} \Psi(x) \tag{1}$$

where $u_c(\mathbf{r})$ and $u_v(\mathbf{r})$ are the atomic-scale periodic parts of the Bloch functions of conduction and valance bands respectively. The term $e^{i\mathbf{K}_{//}^{c,v}\mathbf{r}_{//}}$ is a plane-wave moving perpendicular to the growth direction x with in-plane wave vector $\boldsymbol{\kappa}_{//}$. $\mathbf{r}_{//}$ is a position vector in the quantum-wells' plane. $\Psi(x)$ is the envelope functions that satisfies a Schrödinger-like equation:

$$\frac{-\hbar^2}{2}\frac{\partial}{dx}\left(\frac{1}{m^*}\frac{\partial}{\partial x}\Psi_n(x)\right) + V(x)\Psi_n(x) = E_n\Psi_n(x) \tag{2}$$

where m^* is the effective mass parallel to the growth direction, E_n is the energy at the edge of the n-th subband, and V is the band edge profile potential. The in-plane wavevector $\boldsymbol{\kappa}_{//}$ is set to zero therefore this work is only concerned with carriers with zero in-plane momentum. The effects of nonparabolicity [10] are ignored which require a forth order differential equation under the effective mass approximation [11]. The effects of the band structure are incorporated in the material-dependent parameters E_n and m^*. This equation is discretised either by box method or finite difference method [12] and then solved for the bound states with fixed boundary conditions, or for scattering states with open boundary conditions using transfer matrix method [13]. With finite difference method the partial derivative in the Schrodinger equation is replaced by finite differences over small steps arising from dividing the physical region into subintervals called "mesh steps". This discretization should account for the variation of effective mass across boundaries between the different materials constituting the structure to preserve the continuity of probability current. This requirement was first formulated by BenDaniel and Duke [14] using two boundary conditions at interface x_i between two materials A and B:

$$\Psi_L^A(x_i) = \Psi_R^B(x_i) \tag{3}$$

$$(1/m_A^*)\frac{\partial\Psi_L^A(x_i)}{\partial x} = (1/m_B^*)\frac{\partial\Psi_L^B(x_i)}{\partial x} \tag{4}$$

where Ψ_L^A and Ψ_R^B stands for the envelope function at the left and at the right of an interface x_i between material A and respectively. The discretized version of Schrodinger equation reads:

$$-\frac{\hbar}{2}\left(\frac{2(\Psi_{i+1}-\Psi_i)}{m^*_{i+1/2}\Delta x_i(\Delta x_i+\Delta x_{i-1})} - \frac{2(\Psi_i-\Psi_{i-1})}{m^*_{i-1/2}\Delta x_{i-1}(\Delta x_i+\Delta x_{i-1})}\right) = (E-V_i)\Psi \tag{5}$$

The index denotes a grid point within a one-dimensional mesh. Half integer index represent a point midway between two neighbouring main mesh points and Δx_i is a mesh step between adjacent grid points. Then applying "(5)" at each mesh point gives an eigenvalue equation of the form:

$$A_{\alpha\beta}\Psi_\beta = E\Psi_\alpha \tag{6}$$

which can be readily solved using well developed computer algorithms. The matrix A is a tridiagonal matrix and its inputs contain coefficients from "(4)".

The absorption coefficients [15] are calculated automatically using Fermi's Golden rule:

$$W_{i\to f} = \frac{2\pi}{\hbar}\left|\langle f,k_f|H|i,k_i\rangle\right|\delta(E_f-E_i) \tag{7}$$

which gives the scattering rate for a carrier initially in state $|i, k_i\rangle$ to the final state $|f, k_f\rangle$ through an interaction potential H. A Lorantzian lineshape function has been chosen to approximate the delta function to account for finite transition linewidth due to various scattering mechanisms. The absorption peaks can be controlled easily by adjusting material and simulation parameters via graphical user interface.

The program does not include a self-consistent Schrödinger-Poisson calculation, but instead assumes a stair model in which a linear potential drop across the structure is added using the applied electric field to account for band

bending. This approximation is usually justified in device with lightly doped complex active regions [16].

III. SIMULATION RESULTS AND DISCUSSTION

In this section we present three simulation examples, the first one is used as a validation for the simulator with a previously published results [17] while the second and the third show that the code can be used to address a broad variety of nanoscale structures. The structure sequence of the three coupled well structure is $Al_{0.48}In_{0.52}As/In_{0.53}Ga_{0.47}As$ which creates three coupled quantum wells, with well width of 64 A, 20 A and 19 A respectively, separated by $Al_{0.48}In_{0.52}As$ barrier of width 10 A. Fig.3 shows the lowest four electron's moduli-squared eigen states for this structure calculated with MQWSS.

For the purpose of comparison, the calculated energy values and the corresponding ones reported by Sirtori, et al [17] are given in Table 1. for a single quantum well of 52 A, two coupled quantum wells (wide well 59 A, thin barrier 13 A, narrow well 24 A), and three coupled quantum wells of 46 A, 20 A, 19 A and a barriers of 10 A. In all cases the barrier high was set to 0.52 eV and the effective masses of electrons at the band edges were taken as m_w/m_0=0.043 in the well and m_b/m_0=0.09 in the barrier. Here the subscripts *w* and b denote well and barrier respectively and m_0 the electron rest mass.

From the results of Table 1. we note a difference between our results and Sirtori et al [17]. Clearly the single-band effective mass leads to energies slightly over estimated for higher lying states. This is due to the fact that the effect of remote bands is neglected in the single band model whereas in Sirtori et al [17] work the nonparabolicity effects

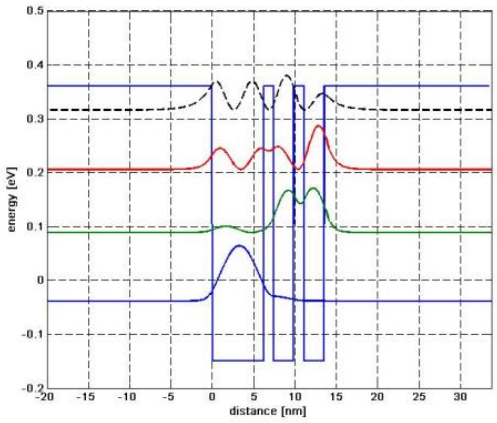

Figure 3. The lowest four electron envelope functions moduli squared and the corresponding eigen energies of an $Al_{0.48}In_{0.52}As/In_{0.53}Ga_{0.47}As$ triple quantum well structure produced by MQWSS.

TABLE I. COMPARISON OF THE ENERGY VALUES OF SINGLE, DOUBLE AND TRIPLE QUANTUM WELL STRUCURE. THE REFEREMCE OF ENERGY IS BAND EDGE OF THE WELL.

Number of Quantum Wells	Eigen Energies [meV]	
	MQWSS	***Sirtori et al* [17]**
Single	111.59, 446.03	123, 381
Double	93.4, 243.8, 420.7	102, 252, 373
Triple	119.6, 235.4, 405.8	126, 242, 383, 494

have been included using Nilson et al [18] model that uses an energy dependent effective mass through :

$$m^*_{w,b}(E) = m^*_{w,b} \cdot (1 + \frac{E - V}{E^{w,b}_g}) \qquad (8)$$

where E^w_g and E^b_g are effective energy gaps and not necessarily match with real energy gaps. Hence "(2)" or equivalently "(6)" is no longer linear eigenvalue problem, rather a nonlinear one in terms of energy [19] and to solve it an iterative algorithm should be invoked. Its known that the effect of Nonparabolicity raises the first subband energy level of any quantum well by a small amount, this is regardless of the well. The consequence of nonparabolicity slightly raises the lowest energy subbands and noticeably shifts down the higher energy subbands [19].

With MQWSS the calculation run in real time whereas with Nilson et al [18] model to achieve a good results the iterative calculation is required until the convergence of effective masses and bound energies , hence obviously it takes a longer time.

The second simulation example is a structure for Quantum Well Infrared Photodetectors (QWIPs). One significant feature of in QWIPs is the ability to operate in two separate wavelength windows by properly tailoring the design of the band gap. This demonstrates the ability to use MQWSS in more sophisticated structure. The simulated structure in this example uses: $(In_{0.53}Ga_{0.47}As)_{0.15}(InP)_{0.85}/In_{0.53}Ga_{0.47}As/(In_{0.53}Ga_{0.47}As)_{0.55}(InP)_{0.452}$ asymmetric step quantum wells material system. The structure consists of $In_{0.53}Ga_{0.47}As$ well, $(In_{0.53}Ga_{0.47}As)_{0.15}(InP)_{0.85}$ step well and $(In_{0.53}Ga_{0.47}As)_{0.55}(InP)_{0.452}$ barrier. The thicknesses of the left and right wells was set to be 25A and 44 A respectively, while the binding/surrounding barrier width was set at 100 A.

The subband energies and the energy wave functions were calculated using the MQWSS at zeros applied electric field are shown in Fig. 4. Fig. 5 shows the absorption spectra (intersubband transition) for the simulated structure. It is observed that the wavelength at which the absorption peaks, reaches its maximum corresponds to the difference in energies between the first and second sublevel available in the well which is 8.745 μm.

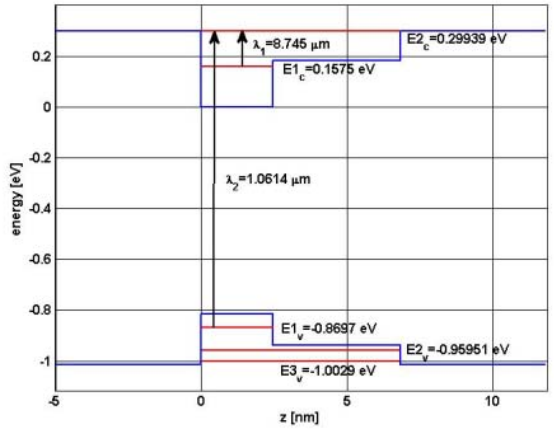

Figure 4. The lowest two electron eigen energies for an $(In_{0.53}Ga_{0.47}As)_{0.15}(InP)_{0.85}/In_{0.53}Ga_{0.47}As$ $/(In_{0.53}Ga_{0.47}As)_{0.55}(InP)_{0.452}$ asymmetric step quantum wells structure produced by our simulator.

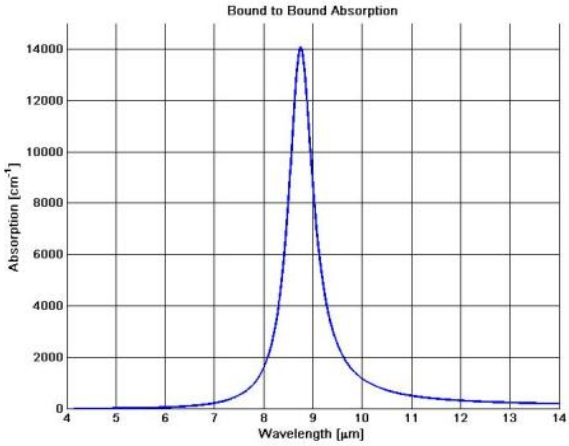

Figure 5. Absorption spectra (intersubband transition) for an $(In_{0.53}Ga_{0.47}As)_{0.15}(InP)_{0.85}/In_{0.53}Ga_{0.47}As$ $/(In_{0.53}Ga_{0.47}As)_{0.55}(InP)_{0.452}$ asymmetric step quantum wells structure produced by MQWSS.

A structure similar to the last one has been studied experimentally by Karunasiri et al [20] made of $Al_{0.44}Ga_{0.56}As$/ $GaAs/A_{l0.18}Ga_{0.82}As$ step quantum well with 60 Å deep well width and 90 Å step well width. The calculated absorption converted to absorbance in order to compare it to [20] is shown in Fig.6. The experimental absorbance is shown in Fig. 7. Both results are given at different bias of 0V, 4V and -4V.

The transitions shown in Fig. 6 are 1-2, 1-3 and 2-3 whereas in Fig. 7 only 1-2 and 1-3 are shown. From Fig. 6 and Fig. 7 we notice a shift in peak positions, which may be due to the difference in effective masses and to the depth of the wells as well as to the experimental error.

Finally the last example is a structure of Quantum Cascade Laser in $GaAs/Al_xGa_{1-x}As$ material system as described in Sirtori et al [21]. For the active region/injector,

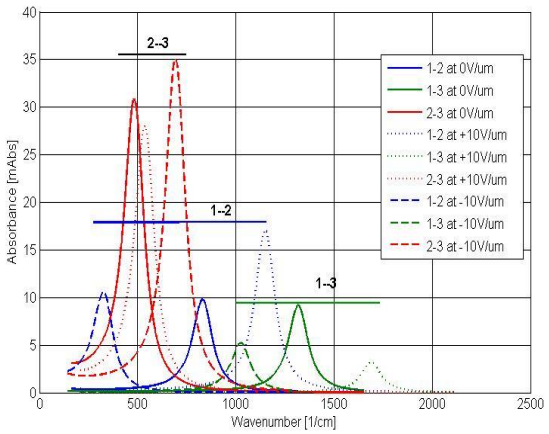

Figure 6. Bound-to-bound absorbance for 1-2, 1-3 and 2-3 transitions in asymmetric step quantum wells structure at diiferent applied electric field produced by MQWSS.

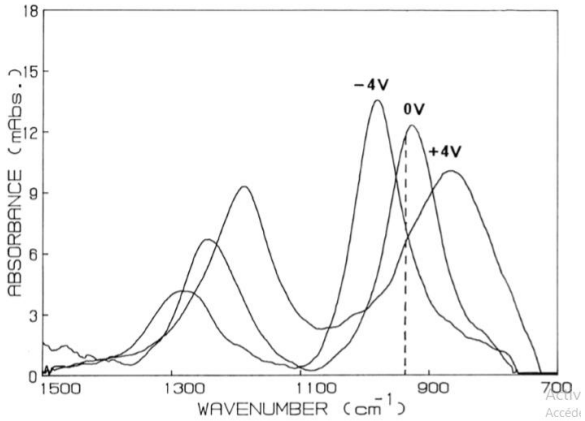

Figure 7. Measured Bound to Bound absorbance for 1-2 and 1-3 transitions in asymmetric step quantum wells structure at diiferent voltage from [21].

$Al_xGa_{1-x}As$ with x=0.33 is used as the barrier material. For more detail about the layer's sequences refer to [21]. The resulting conduction band edge of QCL structure obtained by MQWSS is shown in Fig. 8 along with the corresponding wave functions. The wavy curves represent wave functions shifted by the corresponding bound energies. The transition states are determined based on the dominance of envelope functions which are indicated by black, dashed black and again black respectively from bottom to top in Fig. 8. The calculated transition energies are E_{21}=42 meV and E_{32}=183.2 meV with a difference of ΔE_{21}=4 meV and ΔE_{32}=49.2 meV compared to the reported values from [21]. This difference is due to the effect of nonparabolicity which is ignored here.

IV. CONCLUSION

A simulator for multiple quantum wells structure was presented and implemented with different and flexible material system database and different numerical algorithms. The graphical user interface allows simple and fast operation

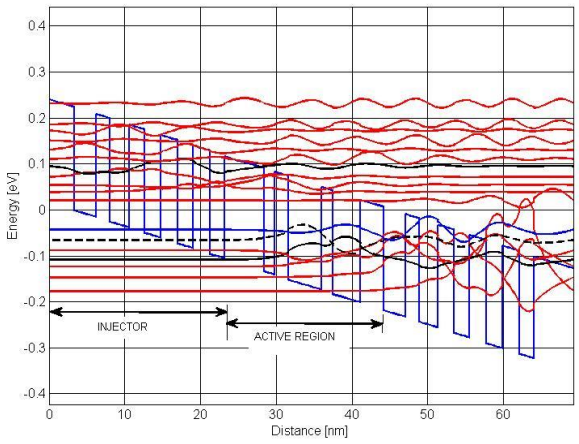

Figure 8. Band edge structure of a GaAs/AlGaAs QCL laser under an applied electric field of 48 kV/cm. The wavy curves are the wave functions. The transition states of active region are bluck, dashed black and black from bottom to top respectively.

of the program while entering complex multiple quantum well structures. As has been shown by the examples, MQWSS can provide useful information using the single band effective mass approximation. However, it is limited in the accuracy of higher energy states.

REFERENCES

[1] S. Agarwal, K. Balamukundhan, N. Neophytou and G. Klimeck, "1D hetero-structure tool for atomistic simulation of nano-devices," Other Nanotechnology Publications, 136, pp. 1, 2008.

[2] K. Barnham, D. Vvedensky, "Low-dimensional Semiconductor Structures", Cambridge University Press, 2001.

[3] P. F. Qiao, S. Mou, S. L. Chuang, "Electronic band structures and optical properties of type-II superlattice photodetectors with interfacial effect," Optics Express 2324, vol. 20, no. 2 Jan 2012.

[4] K. Hackiewicz, T. Manyk, P. Martyniuk, J. Rutkowski, "Theoretical simulation of mid-wave type-II InAs/GaSb superlattice interband cascade photodetector," Proc. SPIE 10404, Infrared Sensors, Devices, and Applications VII, Aug. 2017, 1040404. doi: 10.1117/12.2273421

[5] Z. Stanojevic, O. Baumgartner, "VSP: a Quantum Simulator for Engineering Applications," Society for Micro- and Nanoelectronic, 2013.

[6] G. Bastard, "Superlattice band structure in the envelope-function approximation," *Phys. Rev. B*, vol. 24, no. 10, 1981

[7] W R. Frensley and N G. Einspruch, "Heterostructures and Quantum Devices," VLSI Electronics Microstructure Science, vol. 24, chapter. 1, 1994.

[8] A. Rogalski, P. Martyniuk, and M. Kopytko, "InAs/GaSb type-II superlattice infrared detectors: Future prospect," *Appl. Phys Rev*, vol. 4, no. 3, p. 31304, Sep. 2017.

[9] D. Z. Ting, A. Soibel, A. Khoshakhlagh, L Höglund, S. A. Keo, S. B. Rafol, C. J. Hill, A. M. Fisher, E. M. Luong, J. Nguyen, J. K. Liu, J. M. Mumolo, B. J. Pepper, S. D. Gunapala "Antimonide type-II superlattice barrier infrared detectors," 2017, p. 101770N.

[10] U. Ekenberg, "Nonparabolicity effects in a quantum well : sublevel shift, parallel mass, and landau levels," *Phys. Rev. B*, vol. 40, no. 11, 1989.

[11] C-S. Chang, S. L. Chuang, "Modeling of strained quantum well lasers with spin-orbit coupling," IEEE. *Journal of selected topics in quantum electronics*, vol. 1, no. 2 ,Jun 1995.

[12] I. H. Tan, G. L. Snider, L. D. Chang and E. L. Hu, "A selfconsistent solution of Schrödinger – Poisson equations using a nonuniform mesh," *J. Appl. Phys* vol. 68, no. 8 Oct 1990.

[13] C. Jirauschek, "Accuracy of Transfer Matrix Approaches for Solving the Effective Mass Schrodinger Equation," IEEE Journal of Quantun Electronics, 45(9):1059–1067, 2009.

[14] D.J. BenDaniel, C.B. Duke, Physical Review Letters 152 (1966) 683.

[15] S. L. Chuang, "Physics of Photonic Devices", 2nd ed. (Wiley, New York, 2009), Chap. 4 and 9.

[16] S. L. Chuang, M. S. C. Luo, S. Schmitt-Rink, and A. Pinczuk, "Many-body effects on intersubband transitions in semiconductor quantum-well structures," *Phys.Rec. B* 46, 1897-1899 (1992).

[17] S. Sirtori, F. Capasso and J. Faist, "Nonparabolicity and a sum rule associated with bound-to-bound and bound-to-continuum intersubband transitions in quantum wells," *Phys. Rev. B*, 50(12):8663–921, 1994.

[18] K. D. A. Nelson D F, Miller R C, "Band nonparabolicity effects in semiconductor quantum wells," *Phys. Rev. B*, vol. 35, no. 14, pp. 7770–7773, 1987.

[19] S. Rihani, H. Page, and H. E. Beere, "Quasibound states in semiconductor quantum well structures," *Superlattices Microstruct.*, vol. 47, no. 2, pp. 288–299, 2010.

[20] R.P.G Karunasiri, Y.J. Mii and K.L. Wang, "Tunable infrared modulator and switch using Stark shift in step quantum wells", IEEE Electron. Dev. Lett., 11, pp. 227-229, 1990.

[21] C. Sirtori H. Page, H. E. Beere., "GaAs / Al x Ga 1-x As quantum cascade lasers," *Appl. Phys. Lett.*, vol. 73, no. 24, pp. 3486–3488, 1998.